Simulations of the Vibrational Relaxation of I_2 in Xe

Shenmin Li and Ward H. Thompson*

Department of Chemistry, University of Kansas, Lawrence, Kansas 66045-7582

Received: March 3, 2003; In Final Form: June 17, 2003

The vibrational relaxation of an I_2 molecule in a xenon fluid has been simulated by three methods. The conventional perturbation theory approach based on an equilibrium molecular dynamics (MD) simulation is compared with purely classical nonequilibrium MD and mixed quantum−classical surface-hopping MD simulations. Relaxation times and state-to-state vibrational transition rate constants obtained with these three approaches are compared and information that can be extracted concerning the mechanism of vibrational relaxation is examined. Both harmonic and anharmonic solutes are considered as are some common approximations invoked in obtaining vibrational relaxation times.

1. Introduction

Vibrational energy relaxation (VER), in which a vibrationally excited molecule loses energy to the surrounding solvent, is a critical component of numerous processes in condensed phases.[1,2] Not only does VER play an important role in reaction dynamics and photochemistry, but also it has the potential to be used as a sensitive probe of the environment of the vibrationally excited mode.[3,4] Thus, an accurate theoretical description of VER is vital to modeling chemical dynamics in complex systems. In this paper, we compare three approaches for calculating vibrational relaxation lifetimes: the standard Fermi's Golden rule approach, purely nonequilibrium molecular dynamics simulations, and mixed quantum−classical surface-hopping simulations.

The most common theoretical treatment of VER[5−23] is based on perturbation theory[1,2,24] and makes use of equilibrium molecular dynamics (EMD) simulations. Within this formalism, the state-to-state transition rates are determined by evaluating the Fourier transform of the time correlation function (TCF) of the force exerted by the solvent on the solute vibrational mode at the vibrational frequency of the solute. Given the large number of solvent particles in a condensed-phase system, obtaining the exact quantum mechanical TCF is not feasible except for special cases. Thus, the quantum TCF is usually replaced by its classical analogue,[1] which can be calculated directly during the dynamics simulation. This approach has been widely successful;[1,3,8,15−17,25] however, this classical treatment can fail when the spacing between the solute vibrational states is much larger than k_BT.[10]

One approach to circumventing this problem is to find the relationship between the classical and quantum TCFs, the so-called quantum-correction factor (QCF). In particular, Bader and Berne found an exact analytic form of QCFs for the model system of a harmonic solute bilinearly coupled to a harmonic bath.[5] Furthermore, they pointed out that the VER time for such a system described classically is the same as that obtained from a quantum mechanical treatment. Unfortunately, an exact QCF is generally not known for other systems. Comparing several schemes for obtaining the approximate QCFs for exactly solvable models, Egorov et al.[9] found that no method was satisfactory for all of the models they considered and, more importantly, the performance was inconsistent and the approach is thus not always predictive. Some considerations of how to choose approximate QCFs have been given by Skinner and Park recently.[13] Using a more reliable quantum correction factor, Skinner and co-workers have obtained good agreement with experimental vibrational relaxation lifetimes for O_2 ($n = 1$) in liquid O_2.[11] Most recently, on the basis of the harmonic bath assumption, Kim and Rossky[26] developed a promising approach to obtain a quantum correlation function directly from the simulated classical correlation function. However, because most of these approximate QCFs can only be derived with an effective harmonic bath assumption,[14,26] an anharmonic solvent may represent a significant test.

Recently, a method for calculating the TCF on the basis of Feynman's quantum statistical formulation of path centroid, known as the centroid molecular dynamics method, has been introduced.[27] This method has been applied to a variety of dynamics problems;[28−30] however, its main limitation is that it can only be applied to a certain class of liquid-state correlation functions.[29]

Besides the problem in calculating the force−force TCF, another difficulty associated with the perturbation theory approach is that for high-frequency vibrations an accurate Fourier transform of the TCF is difficult to obtain because of the numerical noise inherent in any computer simulation. However, one can circumvent the numerical Fourier transform by using short time expansions of the force−force TCF. The expansion coefficients are used to determine the parameters of an analytic ansatz for this TCF, which can be evaluated at all times during the MD simulation and through which the Fourier transform of the TCF can be obtained analytically. Egorov and Skinner expanded the TCF in powers of time up to t^4 and calculated the vibrational relaxation rates of I_2 ($n = 1$) in xenon.[8] The results are expected to be significantly better than those obtained by Gaussian expansion (up to t^2) method (see section 4.1).

Nonequilibrium molecular dynamics (NEMD) provides a direct, nonperturbative, purely classical approach for calculating VER rates in solution. The NEMD method has been applied to a variety of condensed-phase systems.[16,17,31−33] Some results

* To whom correspondence should be addressed. E-mail: wthompson@ku.edu. Fax: 785-864-5396.

10.1021/jp0345452 CCC: $25.00
Published on Web 09/20/2003

for which NEMD VER rates are comparable to those obtained by the EMD method have been discussed by Bader and Berne.[5]

In addition to the EMD-based perturbation theory approach and the purely classical NEMD simulations mentioned above, an alternative approach for exploring dynamics in solution is based on Tully's surface-hopping method.[34,35] Unlike the quantum−classical incarnation of the standard EMD-based treatment,[1,5] the surface-hopping approach is not based on perturbation theory. Therefore, the weak coupling approximation is not invoked, quantum mechanical effects associated with the solute are included, and numerical problems, for example, associated with the Fourier transform, are circumvented. In addition, the surface-hopping approach accounts for self-consistent interaction of the quantum and classical subsystems. Thus it provides an additional context in which to investigate the potential shortcomings of mixed quantum−classical methods.[5] Moreover, the MQC surface-hopping simulations represent an alternative approach for exploring the mechanisms of VER more directly than perturbation theory, for example, how the energy is deposited in the surrounding bath.

The VER of I_2 in xenon has been widely studied by experiments[36,37] and theory.[8,20,22,38−42] In particular, the vibrational relaxation of I_2 in xenon has been well-characterized experimentally by Harris and co-workers for a range of solvent temperatures and densities. Brown et al.[38] carried out NEMD simulations to model these experiments.[36,37] Their results for the decay of I_2 vibrational energy are in very good agreement with the experimental results if the time axis of molecular dynamics decay is scaled by a factor of ∼12. The significantly more rapid energy transfer in the simulations was attributed to a too-repulsive I_2−Xe potential. With the use of the same intermolecular potentials, similar VER times were obtained with the instantaneous-pair theory developed by Larsen and Stratt.[42] The idea of this theory is that the main contribution to vibrational friction correlation comes from a few mutual nearest-neighbor pairs between individual solute and solvent sites. Their results suggest that the vibrational relaxation of I_2 in xenon is a few-body dynamics process. Egorov and Skinner have calculated vibrational relaxation times, T_1, over a wide range of densities and temperatures.[8] They obtained good agreement between their results, based on a breathing sphere model, and T_1 values extracted from experimental data[36] by fitting one parameter in the interaction potential.[43] In their study, the force−force TCF was fit using short-time information up to order t^4. More recently, Miller and Adelman calculated the temperature and solvent density dependence of the vibrational energy relaxation rate constant, $k(T,\rho)$.[20] Their VER times are obtained based on a Gaussian approximation for the force−force TCF, which is exact to order t^2. No comparison with experiments is given. The Gaussian approximation, while perhaps yielding significant absolute errors in T_1 (see section 4.1), will probably often reliably predict experimental trends.

In this paper, the standard MQC surface-hopping method, NEMD simulations, and EMD simulations based on perturbation theory are carried out for I_2 in a xenon fluid. Vibrational relaxation times obtained by these three kinds of molecular dynamics simulations and mechanistic information obtained by the MQC and EMD simulations are compared and discussed. The organization of this paper is as follows. In section 2, we describe how VER is simulated in each of these three methods. The details of the computational procedures are given in section 3, and the calculated results are presented and discussed in section 4. Finally, a brief summary is offered in section 5.

2. Theory

2.1. Equilibrium Molecular Dynamics (EMD). The most prevalent approach for calculating vibrational relaxation rate constants is based on perturbation theory and requires only an equilibrium molecular dynamics simulation. As discussed in the Introduction, straightforward application of Fermi's Golden rule can be problematic for real systems because of the difficulty in knowing the proper quantum correlation function. One successful case for which the state-to-state vibrational transition rate constant has been derived is that of a harmonic oscillator solute with a harmonic solvent bath and solute−solvent coupling that is linear in the solute coordinate.[5] Under these assumptions, the state-to-state transition rate from state n to state $n-1$ can be written as[5]

$$k^{\mathrm{qm}}_{n-1\leftarrow n} = \frac{2n}{\mu\beta\hbar\omega[1+\exp(-\beta\hbar\omega)]}\xi'_{\mathrm{qm}}(\omega) \tag{1}$$

where $\xi'_{\mathrm{qm}}(\omega)$ is the frequency-dependent quantum dynamic friction and μ is the reduced mass of the solute molecule. The friction, $\xi'_{\mathrm{qm}}(\omega)$, can be determined analytically from its classical analogue and a QCF,

$$\xi'_{\mathrm{qm}}(\omega) = \frac{\beta\hbar\omega}{2}\coth\left(\frac{\beta\hbar\omega}{2}\right)\xi'_{\mathrm{cl}}(\omega) \tag{2}$$

with the classical dynamic friction given by

$$\xi'_{\mathrm{cl}}(\omega) = \beta\int_0^\infty \mathrm{d}t\,\cos(\omega t)\,\langle\delta F(t)\delta F(0)\rangle_{\mathrm{cl}} \tag{3}$$

The classical force autocorrelation function, $\langle\delta F(t)\delta F(0)\rangle_{\mathrm{cl}}$, where $\delta F(t) = F(t) - \langle F\rangle$ and F is the force exerted by the solvent on the solute bond, is calculated during a purely classical molecular dynamics simulation carried out with a fixed solute bond distance.

Using a kinetic scheme and detailed balance, Bader and Berne showed that the vibrational energy relaxation obeys an exponential decay law and that the relaxation rate constant, T_1^{-1}, in a mixed quantum−classical treatment (a quantum solute in a classical solvent) can be written as

$$T_1^{-1} = \frac{\tanh(\beta\hbar\omega/2)}{\beta\hbar\omega/2}\frac{\xi'_{\mathrm{cl}}(\omega)}{\mu} \tag{4}$$

For a quantum solute in a quantum solvent,

$$T_1^{-1} = \frac{\xi'_{\mathrm{cl}}(\omega)}{\mu} \tag{5}$$

which is the same as the purely classical result. (It is interesting to note that using eqs 1 and 2, one can easily obtain the VER time T_1 (eq 5) in terms of the state-to-state transition rate constants as

$$T_1 = (k_{0\leftarrow 1} - k_{1\leftarrow 0})^{-1} \tag{6}$$

which is in agreement with that derived by Landau and Teller.[44]) Obviously, the assumptions of a harmonic solute, a harmonic solvent bath, and weak bilinear coupling mean these equations are approximate for realistic systems. However, for this infinitely dilute rare gas solution system (I_2 in xenon), we use this QCF without test; we expect that the anharmonicity of the solvent is not too large.

2.2. Nonequilibrium Molecular Dynamics. Nonequilibrium molecular dynamics can be used to determine classical vibra-

tional energy relaxation times directly by investigating the time decay of excess vibrational energy. If the energy decay is exponential, the relaxation time T_1 is given by

$$\frac{\langle E_v(t)\rangle - \langle E_v(\infty)\rangle}{\langle E_v(0)\rangle - \langle E_v(\infty)\rangle} = e^{-t/T_1} \tag{7}$$

where $\langle E_v(t)\rangle$ is the nonequilibrium average of the vibrational energy at time t, $\langle E_v(\infty)\rangle$ is the equilibrium average vibrational energy, and the nonequilibrium average initial energy is $\langle E_v(0)\rangle$. In the present work, the vibrational energy for a diatomic solute is taken to be

$$E_v(t) = \frac{p_r^2(t)}{2\mu} + V[r(t)] \tag{8}$$

where r is the diatom internuclear distance with conjugate momentum p_r and $V(r)$ is the potential energy function for an isolated diatom.

2.3. MQC Surface-Hopping Approach. A nonequilibrium mixed quantum−classical surface-hopping approach can also be used to calculate relaxation times.[45−48] Here we consider one solute molecule dissolved in a solvent of N atoms. The details of our implementation of vibrationally adiabatic molecular dynamics have been given elsewhere.[34,49] Briefly, the classical Hamiltonian for the full system is

$$H(r,p_r,\mathbf{e},\mathbf{p}_e,\mathbf{Q},\mathbf{P},) = \frac{p_r^2}{2\mu} + \frac{\mathbf{p}_e^2}{2\mu r^2} + \sum_{j=1}^{N}\frac{\mathbf{P}_j^2}{2m_j} + V(r,\mathbf{e},\mathbf{Q}) \tag{9}$$

where r and $\mathbf{e}$ are the bond distance and orientation coordinates of the solute molecule, $\mathbf{Q} = (\mathbf{Q}_1, \mathbf{Q}_2, ..., \mathbf{Q}_N)$ are the coordinates of the N solvent atoms, p_r, $\mathbf{p}_e$, and $\mathbf{P} = (\mathbf{P}_1, \mathbf{P}_2, ..., \mathbf{P}_N)$ are the corresponding momenta, μ is the solute reduced mass, and m_j is the mass of solvent atom j. The potential energy, $V(r,\mathbf{e},\mathbf{Q})$, is the sum of the vibrational potential of the solute and the pairwise Lennard-Jones potentials describing the solute−solvent and solvent−solvent interactions. Within the mixed quantum−classical formalism, the vibrational degree-of-freedom of the solute is treated quantum mechanically while the remaining degrees-of-freedom are treated classically. If a Born−Oppenheimer separation between the "fast" vibration and the other, "slow," coordinates is valid, the dynamics of the system is then governed by the following coupled equations: first, the vibrational Schrödinger equation,

$$\hat{h}_r(\mathbf{e},\mathbf{p}_e,\mathbf{Q})\phi_n(r;\mathbf{e},\mathbf{p}_e,\mathbf{Q}) = E_n(\mathbf{e},\mathbf{p}_e,\mathbf{Q})\phi_n(r;\mathbf{e},\mathbf{p}_e,\mathbf{Q}) \tag{10}$$

from which the stationary adiabatic vibrational states, $\phi_n(r;\mathbf{e},\mathbf{p}_e,\mathbf{Q})$, of the solute for fixed classical coordinates $\mathbf{e}$, $\mathbf{p}_e$, and $\mathbf{Q}$ are obtained, where the quantum mechanical Hamiltonian is written as

$$\hat{h}_r(\mathbf{e},\mathbf{p}_e,\mathbf{Q}) = \frac{\hat{p}_r^2}{2\mu} + \frac{\mathbf{p}_e^2}{2\mu\hat{r}^2} + V(\hat{r},\mathbf{e},\mathbf{p}_e,\mathbf{Q}) \tag{11}$$

and, second, the classical equations of motion governed by the vibrationally adiabatic Hamiltonian for state n,

$$H_n(\mathbf{e},\mathbf{p}_e,\mathbf{Q},\mathbf{P}) = \sum_{j=1}^{N}\frac{\mathbf{P}_j^2}{2m_j} + \langle\phi_n|\hat{h}_r|\phi_n\rangle_r = \sum_{j=1}^{N}\frac{\mathbf{P}_j^2}{2m_j} + E_n(\mathbf{e},\mathbf{p}_e,\mathbf{Q}) \tag{12}$$

The time-dependent wave function, $\Psi(r,\mathbf{e},\mathbf{p}_e,\mathbf{Q},t)$, can be expanded in terms of an orthonormal adiabatic basis, $\phi_k(r;\mathbf{e},\mathbf{p}_e,\mathbf{Q})$,

$$\Psi(r,\mathbf{e},\mathbf{p}_e,\mathbf{Q},t) = \sum_k C_k(t)\phi_k(r;\mathbf{e},\mathbf{p}_e,\mathbf{Q}) \tag{13}$$

Then, the complex-valued expansion coefficients C_k satisfy

$$i\hbar\dot{C}_k = \sum_{j=1} C_j(E_k\delta_{kj} - i\hbar\dot{\mathbf{Q}}\cdot\mathbf{d}_{kj}) \tag{14}$$

where E_k is the energy of the adiabatic vibrational state k obtained by solving eq 10, $|C_k|^2$ is the corresponding occupation probability, and $\mathbf{d}_{kj}(\mathbf{e},\mathbf{p}_e,\mathbf{Q})$ is the nonadiabatic coupling vector defined as

$$\mathbf{d}_{kj}(\mathbf{e},\mathbf{p}_e,\mathbf{Q}) = \langle\phi_k(r;\mathbf{e},\mathbf{p}_e,\mathbf{Q})|\nabla_{\mathbf{Q}}\phi_j(r;\mathbf{e},\mathbf{p}_e,\mathbf{Q})\rangle_r \tag{15}$$

Tully's "fewest switches" algorithm[34,35] is used to incorporate transitions between the different adiabatic vibrational surfaces induced by the nonadiabatic coupling. A random number ξ ($0 < \xi < 1$) is generated and compared with the transition probability g_{kj} between the adiabatic states k and j at each classical time step. The transition probability is given by

$$g_{kj} = \max\left(0,\frac{b_{jk}\delta t}{a_{kk}}\right) \tag{16}$$

where

$$a_{kk} = |C_k|^2$$
$$b_{jk} = -2\mathrm{Re}\{C_jC_k^*(\dot{\mathbf{Q}}\cdot\mathbf{d}_{jk})\} \tag{17}$$

For a two-level system, for instance, if $k = 1$, a switch to state 2 will occur if $\xi < g_{12}$ and if $k = 2$, a switch to state 1 will occur if $\xi < g_{21}$. To maintain energy conservation, if a switch does occur, the classical velocities are scaled. If a hop is attempted to a state of high energy and the required velocity reduction is greater than the component of the velocity to be adjusted, the velocity component is reversed without switching states.[34]

The standard MQC method just described retains full coherence in the evolution of quantum amplitudes, which is supposed to overestimate the quantum subsystem−bath nonadiabatic coupling, as discussed by Rossky and co-workers.[50,51] In a series of papers, they pointed out that the coherence loss (quantum decoherence effect) attributed to the subtle differences in the dynamics between the bath and different quantum states of the subsystem can be important in determining the rate of electronic transitions. Several explicit methods of incorporating decoherence effects in mixed quantum−classical systems were suggested to improve the calculated rate constants.

Unlike electronically nonadiabatic systems, which often have only small regions with strong nonadiabatic coupling (the solvated electron being an exception) where transitions can occur, here a vibrational transition can occur at any time during the whole dynamics process because while the nonadiabatic

TABLE 1: Potential Parameters of I_2 in Xenon

		I−Xe	Xe−Xe	I−I
Lennard-Jones	σ (Å)	3.94	4.10	
	ϵ (K)	323.7	221.6	
Morse	D_e (eV)			1.547
	α (Å^{-1})			1.864
	r_0 (Å)			2.667
harmonic	k (eV)			2.993
	r_0 (Å)			2.667

coupling continually fluctuates, no extended weak nonadiabatic coupling region can be identified. For example, there is an average of 80 transitions during the two-level model 500 ps MQC simulation of the present system. Therefore, at short times, the quantum states associated with different possible classical trajectories retain coherence; however, as the various possible classical trajectories diverge, coherence is dissipated.

Here we use the surface-hopping approach with no special accounting for decoherence effects beyond averaging over the random seed that determines the hops. While the effect on vibrational relaxation times is not clear, it is the logical starting point; we are currently investigating methods for incorporating decoherence in MQC simulations of vibrational relaxation.

3. Simulation Details

The system considered in this work is a single I_2 solute dissolved in a solvent of 107 xenon atoms in a cubic box of length 19.87 Å with the minimum image convention and periodic boundary conditions,[52] corresponding to a solvent density of 3.0 g/cm^3. Constant energy (*NVE*) molecular dynamics simulations are carried out with an average temperature of ~303 K during the EMD and MQC simulations. For the NEMD simulations, the situation is more complicated. To examine the VER of the I_2 vibrational mode, energy is added to the I_2 vibrational mode at the beginning of the data collection stage. Because this procedure is after an equilibration stage, the average temperature of the system in this data collection stage can be difficult to control. To compare VER times with the other two methods, we use constant temperature (*NVT*) molecular dynamics for the two low initial excitation energy (ΔE_0 = 214 and 321 cm^{-1}) simulations. For the two high initial excitation energy (ΔE_0 = 6000 and 9000 cm^{-1}) NEMD simulations, constant energy molecular dynamics were used. We have found that for the high initial energies, the temperature fluctuations do not strongly affect the energy decay.

The solute−solvent and solvent−solvent interactions are described by a sum of pairwise Lennard-Jones potentials. To study the effect of the solute potential on vibrational energy relaxation, both Morse and harmonic oscillator potentials are used to describe the solute molecule vibration during the NEMD and MQC simulations. The potential parameters are given in Table 1.

3.1. EMD Simulations. Constant energy (*NVE*) molecular dynamics simulations are carried out using a leapfrog Verlet integrator[52] with the I_2 bond length constrained to its equilibrium value. (The equations of motion for the rigid I_2 diatomic are integrated directly.[52]) The average temperature during the simulations is 304.3 K. The force exerted by the solvent atoms along the I_2 bond is monitored at each MD time step and the force−force TCF is then calculated. The force used in eq 3 is given by

$$F = \frac{1}{2}(\mathbf{F}_{Ia} - \mathbf{F}_{Ib})\cdot\hat{\mathbf{n}} \tag{18}$$

where $\mathbf{F}_{Ia}$ and $\mathbf{F}_{Ib}$ are the forces exerted by the solvent on the two solute iodine atoms and $\hat{\mathbf{n}}$ is the unit vector between them. The power spectrum of the TCF evaluated at the I_2 gas-phase vibrational frequency ($\hbar\omega_0$ = 214 cm^{-1}) is obtained by the standard fast Fourier transform technique. To obtain converged results, an ensemble average of 35 trajectories is calculated with step size of 2 fs and a propagation time of 625 ps.

3.2. NEMD Simulations. Constant temperature (*NVT*) molecular dynamics simulations by the constraint method[52] are carried out for both the anharmonic and harmonic solute models with two low initial excitation vibrational energy values, ΔE_0 = 214 and 321 cm^{-1}, which correspond to the vibrational energy of the I_2 molecule in the n = 1 excited state without and with the vibrational zero-point energy, respectively. A trajectory is first propagated using a leapfrog Verlet integrator[52] (δt = 3 fs) for a 60 ps equilibration period; the solute vibrational energy is then increased by ΔE_0 from an average equilibrium vibrational energy k_BT. All excess energy is added as kinetic energy by setting the bond distance to be the gas-phase equilibrium value; the center-of-mass and orientation are not changed. Next, a 900 ps nonequilibrium trajectory is run for data collection. An additional 10 ps equilibration period is performed before another nonequilibrium trajectory is run. This procedure is repeated for a total of 700 nonequilibrium trajectories. Finally, the average energy is fit to eq 7 to check the energy decay law and to get the relaxation time T_1. Instead of constant temperature dynamics simulations, constant energy dynamics simulations are used for two high initial vibrational energy values, ΔE_0 = 6000 and 9000 cm^{-1}, while the other simulation parameters and procedures are the same as those for the low excitation energy simulations. For both anharmonic and harmonic solute systems, the average temperatures are 326 and 342 K for ΔE_0 = 6000 and 9000 cm^{-1}, respectively, during the simulations.

3.3. MQC Simulations. The MQC simulations have been carried out including two and three vibrationally adiabatic states (two-level model and three-level model) to investigate the vibrational energy relaxation. The simulation is initiated with an equilibration period consisting of classical (with a fixed I_2 bond distance) and adiabatic mixed quantum−classical dynamics in the n = 1 state of 50 ps (δt = 2.5 fs) and 20 ps (δt = 2 fs), respectively.[49] A swarm of trajectories is then propagated, all starting from the final equilibrated configuration, for 500 ps under constant energy (*NVE*) surface-hopping dynamics during which the data is collected for analysis. At each classical dynamics step, the vibrational Schrödinger equation (eq 10) is solved by an iterative Lanczos algorithm.[53,54] This approach can be tuned for the number of states of interest. For example, for this system, only the three and four lowest vibrational states are calculated for the two-level and three-level model, respectively, to meet the convergence criterion. A potential optimized discrete variable representation (PO-DVR) basis[55,56] is also used to decrease the computational expense; 30 PO-DVR basis functions are used here. The populations of the vibrational states are obtained by averaging over 450 MQC trajectories with a step size of 2 fs. These 450 trajectories consist of 15 swarms of trajectories, each with a different equilibration run; each swarm of trajectories contains 30 trajectories from the same equilibration run but with different random number sequences, which determine the vibrational transitions by Tully's "fewest switches" surface-hopping algorithm as described in section 2.3.

4. Results and Discussion

4.1. EMD Simulations. The normalized force autocorrelation function obtained from EMD simulations is shown in Figure 1.

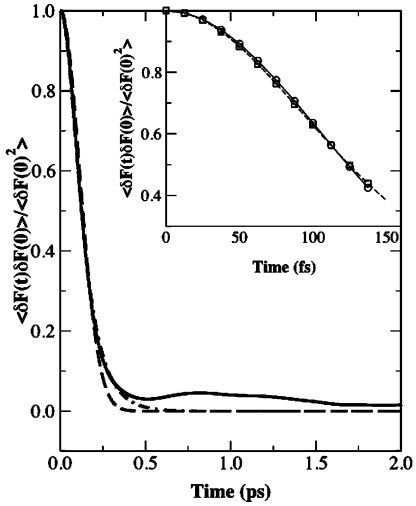

Figure 1. Normalized force autocorrelation function as a function of time. The solid, dashed, and dotted-dashed lines represent numerical results, a Gaussian fit, and a fit of order t^4 given in eq 21, respectively. The numerical results and fits are shown for short times (up to 150 fs) in the inset with squares (Gaussian fit) and circles (order t^4 fit).

TABLE 2: Overall and State-to-State Vibrational Relaxation Times

		T_1 (ps)		$k_{0\leftarrow1}^{-1}$ (ps)	
		anharmonic solute	harmonic solute	anharmonic solute	harmonic solute
NEMD	$\Delta E_0 = 214$ cm^{-1}	185	112		
	$\Delta E_0 = 321$ cm^{-1}	169	116		
	$\Delta E_0 = 6000$ cm^{-1}		110		
	$\Delta E_0 = 9000$ cm^{-1}		98		
EMD	cl−cl		149		
	q−cl		162		102
	q−q		149		94
MQC	two-level	114	88	155	120
	three-level	132	113		

The correlation function decays rapidly at short times (~250 fs) but displays a small long-time tail beyond 2 ps. The vibrational relaxation time T_1 and state-to-state transition rate constant $k_{0\leftarrow1}$ are calculated from this autocorrelation function according to eqs 4 and 5 and eq 1, respectively. We have adopted Berne's harmonic model[5] here in the absence of formulations for a general anharmonic system; it is anticipated that the anharmonicity of the xenon solvent will be small. The quantum correction factor in these equations provides a method for connecting purely classical, mixed quantum−classical, and purely quantum mechanical relaxation times and rate constants obtained from perturbation theory for the harmonic system described in section 2.1; the results are listed in Table 2. For the I_2 molecule at $T \approx 300$ K, we have $\hbar\omega \approx k_B T$ and the QCF, for example, in eq 2, is approximately 1 (here $(\beta\hbar\omega/2)\coth(\beta\hbar\omega/2) \cong 1.08$). Thus the classical, quantum, and mixed quantum−classical EMD relaxation times are all similar. A comparison of rate constants and VER times obtained from the three methods considered in this paper is postponed to section 4.4.

To examine the short-time approximations and compare with the results of Miller and Adelman,[20] we fit the normalized force−force TCF with a Gaussian (shown as a dashed line in Figure 1),

$$\frac{\langle F(0)F(t)\rangle}{\langle F(0)^2\rangle} = \exp\left(-\frac{t^2}{2\tau^2}\right) \tag{19}$$

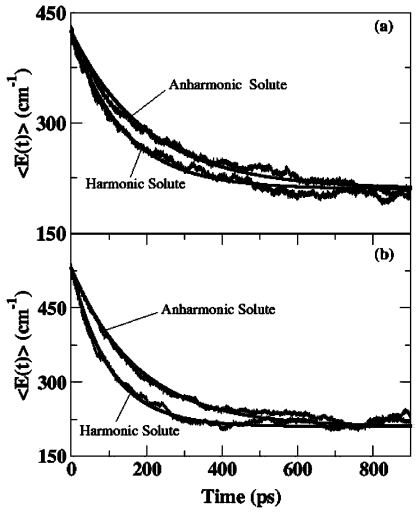

Figure 2. The vibrational energy relaxation of I_2 in xenon from the NEMD simulations using both harmonic and anharmonic solute potentials versus time for initial vibrational excitation energies of (a) $\Delta E_0 = \hbar\omega = 214$ cm^{-1} and (b) $\Delta E_0 = 3\hbar\omega/2 = 321$ cm^{-1}. The smooth lines are exponential fits based on eq 7.

This fit yields $\tau = 112$ fs, which is nearly the same as the comparable result of Miller and Adelman ($\tau = 112.68$ fs). The analytic VER time T_1 is then given by

$$T_1 = \frac{2\mu}{\beta\langle F(0)^2\rangle}\left(\frac{1}{2\pi\tau^2}\right)^{1/2}\exp(\omega_0^2\tau^2/2) \tag{20}$$

which yields $T_1 = 7.3$ ns; this is much larger than the $T_1 = 149$ ps obtained from the numerical Fourier transform. However, it is in good agreement with the result of Miller and Adelman ($T_1 = 7.64$ ns).

We have also fit the TCF to an analytic form based on an expansion up to order t^4 according to an approach used by Egorov and Skinner[8] (dashed−dotted line in Figure 1),

$$\frac{\langle F(0)F(t)\rangle}{\langle F(0)^2\rangle} = \frac{\cos(bt)}{\cosh(at)} \tag{21}$$

Using this approach, we found T_1 to be 43.4 ps based on eq 31 of ref 7. Naturally, the fit to order t^4 is better than that to order t^2 especially for the very short times. The force autocorrelation function and two fits are shown for the first 150 fs in the inset panel of Figure 1. Note that the order t^4 fit is indistinguishable from the numerical result on this time scale, while the Gaussian approximation is in good agreement but with clear differences. However, at longer times, both the Gaussian approximation and the fit to order t^4 are inadequate for describing the decay of the calculated autocorrelation function because they fall too rapidly to zero.

4.2. NEMD Simulations. The vibrational energy relaxation of I_2 from the NEMD simulations is shown as a function of time in Figure 2. Results are presented for both harmonic and anharmonic I_2 potentials and two initial excitation energies ($\Delta E_0 = 214$ and 321 cm^{-1}). The vibrational energy is fit to the exponential decay law in eq 7 to extract the vibrational relaxation time T_1; these times are given in Table 2. It is not clear to us how one would unambiguously extract state-to-state transition rate constants from these simulations, and we have not attempted to do so. It can be seen from Figure 2 that the vibrational energy relaxation does obey an exponential decay law, in accord with eq 7, for both harmonic and anharmonic solute potentials with these low initial excitation energies.

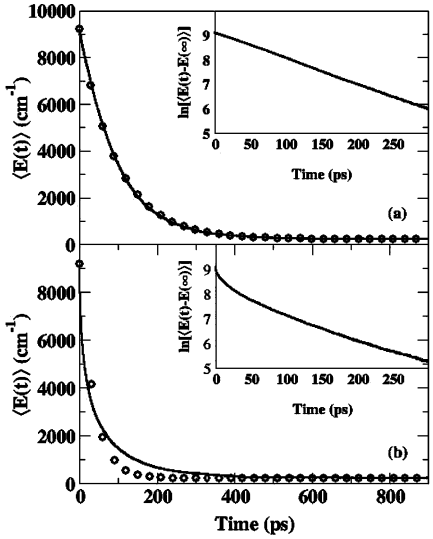

Figure 3. Vibrational energy relaxation of I_2 in xenon as a function of time for (a) a harmonic and (b) an anharmonic solute potential from the NEMD simulations. The initial vibrational excitation energy of the solute is 9000 cm^{-1}. The circles show the exponential fits. The natural logarithm of the excess vibrational energy is shown as a function of time for the two simulations in the insets with the equilibrium vibrational energy, $E_v(\infty)$, taken to be 210 cm^{-1}.

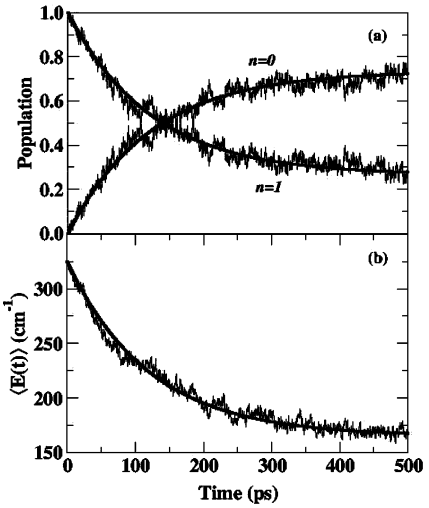

Figure 4. The results of two-level model MQC simulations of I_2 in xenon shown in two ways: (a) the population of the adiabatic vibrational states ($n = 0,1$) as a function of time; (b) vibrational energy relaxation as a function of time. Results are shown for the anharmonic solute potential. The smooth lines are fits based on eqs 23 and 24.

Results are presented for a high initial excitation energy ($\Delta E_0 = 9000$ cm^{-1}) in Figure 3 for the harmonic and anharmonic I_2 potentials, along with exponential fits; the corresponding relaxation times for the harmonic potential are given in Table 2. In this case it is obvious that, for the anharmonic solute, the energy decay *does not* obey an exponential decay law when the initial excitation is large ($\Delta E_0 = 6000$ cm^{-1}, not shown, and 9000 cm^{-1}). This is illustrated both by the inadequate exponential fit and the nonlinearity of $\ln[\langle E(t) - E(\infty)\rangle]$ versus time shown in the inset. Taken together, the results presented in Figures 2 and 3 indicate that, not surprisingly, at low initial energies the anharmonicity of the solute is less prominent but with high initial energy this is not the case and the solute anharmonicity leads to energy decay that cannot be adequately described by only one parameter such as T_1. This has been noted previously by others.[8,57] In addition, the nonexponential (or multiexponential) energy decay is consistent with the experimental results of Paige and Harris[36,37] and the previous NEMD simulations of Brown et al.[38] In fact, our NEMD results appear to be in very good agreement with the latter simulations.

The energy relaxation times T_1 obtained from the NEMD simulations (see Table 2) with low initial vibrational excitation, $\Delta E_0 = 214$ and 321 cm^{-1}, are ~112 and 116 ps for the harmonic solute, respectively, while for the anharmonic solute, they are ~185 and 169 ps, respectively. Thus, the VER times for the anharmonic solute are longer than those for the harmonic one. A more thorough comparison of the harmonic and anharmonic solutes is given in section 4.5. For the two high initial vibrational excitation energies, $\Delta E_0 = 6000$ and 9000 cm^{-1}, of the harmonic solute the VER times T_1 are ~110 and 98 ps, respectively; as noted above, a single relaxation time cannot be obtained for the anharmonic solute at these energies. Note that the relaxation times are essentially independent of the initial excitation energy for the harmonic solute systems with both low and high initial energies, taking into account that the temperatures are higher in the high initial energy simulations than the low excitation energy simulations (as discussed in section 3.2). A weak dependence of the relaxation times on the initial excitation energy is found in anharmonic solute simulations with low initial vibrational energy. It is not clear what is the proper choice of vibrational excitation energy to simulate, for example, $n = 1$ relaxation, $\Delta E_0 = 214$ or 321 cm^{-1}, and the dependence of T_1 on the initial energy further complicates this issue.

4.3. MQC Simulations. One of the parameters in the MQC approach described in section 2.3 is the number of vibrationally adiabatic states included in the simulation. For the vibrational relaxation of I_2 ($n = 1$), the simplest possible choice is two states (two-level model). The VER time T_1 is expected to be inaccurate in this model, but information regarding transitions between the $n = 1$ and $n = 0$ levels can still be obtained from this two-level model. Therefore, we will concentrate on the two-level model in the following. We have carried out preliminary calculations involving three states and comment on these in section 4.4.

Using the MQC surface-hopping approach described in section 2.3, we calculate the populations of the $n = 1$ and $n = 0$ vibrational states as a function of time. The results from these simulations are plotted in Figure 4. For this two-state system, the vibrational energy relaxation obeys an exponential decay law for both harmonic and anharmonic solutes, and thus, the vibrational relaxation time, T_1, can be found by fitting the vibrational state populations or, alternatively, the energy relaxation directly. Obtaining the state-to-state transition rate constants, $k_{1\leftarrow 0}$ and $k_{0\leftarrow 1}$, requires additional consideration.

The two-level model assumes that the transitions only occur between the lowest two solute vibrational states. From the kinetic scheme

$$n = 1 \underset{k_{1\leftarrow 0}}{\overset{k_{0\leftarrow 1}}{\rightleftharpoons}} n = 0 \tag{22}$$

and an initial population in the excited state, $\rho_1(0) = 1$, the population as function of time is given by[58]

$$\langle \rho_1(t)\rangle = \frac{k_{1\leftarrow 0} + k_{0\leftarrow 1}\exp[-(k_{1\leftarrow 0} + k_{0\leftarrow 1})t]}{k_{1\leftarrow 0} + k_{0\leftarrow 1}}$$

$$\langle \rho_0(t)\rangle = 1 - \langle \rho_1(t)\rangle \tag{23}$$

The average vibrational energy as a function of time t is given by

$$\langle E(t)\rangle = \left\langle \sum_{i=0,1} \epsilon_i(t)\rho_i(t) \right\rangle = \langle [\epsilon_1(t) - \epsilon_0(t)]\rho_1(t)\rangle - \langle \epsilon_0(t)\rangle \tag{24}$$

which can be obtained directly from the MQC surface-hopping simulation. To fit $\langle E(t)\rangle$ and extract the transition rate constants, we use eqs 23 and 24 assuming in the latter that, for example, $\langle \epsilon_1(t)\rho_1(t)\rangle = \langle \epsilon_1(t)\rangle\langle \rho_1(t)\rangle$ and $\langle \epsilon_1(t)\rangle = \langle \epsilon_1\rangle_{eq} \equiv \epsilon_1$. This gives the nonequilibrium vibrational energy in terms of the state-to-state rate constants as

$$\langle E(t)\rangle = \frac{\epsilon_0 k_{0\leftarrow 1} + \epsilon_1 k_{1\leftarrow 0}}{k_{0\leftarrow 1} + k_{1\leftarrow 0}} + \frac{(\epsilon_1 - \epsilon_0)k_{0\leftarrow 1}}{k_{0\leftarrow 1} + k_{1\leftarrow 0}} \, e^{-(k_{0\leftarrow 1} + k_{1\leftarrow 0})t} \tag{25}$$

According to detailed balance, $k_{1\leftarrow 0} = k_{0\leftarrow 1}\, e^{-\beta(\epsilon_1 - \epsilon_0)}$, so the average energy can be written as

$$\langle E(t)\rangle = \frac{\epsilon_0 + \epsilon_1 e^{-\beta(\epsilon_1 - \epsilon_0)}}{1 + e^{-\beta(\epsilon_1 - \epsilon_0)}} + \frac{\epsilon_1 - \epsilon_0}{1 + e^{-\beta(\epsilon_1 - \epsilon_0)}} \, e^{-k_{0\leftarrow 1}[1 + \exp(-\beta(\epsilon_1 - \epsilon_0))]t} \tag{26}$$

where the first term on the right-hand side is the equilibrium average vibrational energy of the solute. Clearly the energy relaxation obeys an exponential decay law with the relaxation time T_1 given by

$$T_1 = (k_{1\leftarrow 0} + k_{0\leftarrow 1})^{-1} = [k_{0\leftarrow 1}(1 + e^{-\beta(\epsilon_1 - \epsilon_0)})]^{-1} \tag{27}$$

This is obviously in contrast to eq 6, obtained for a harmonic solute bilinearly coupled to a harmonic bath.[5] Note that eq 27 is derived by assuming that only the $n = 0$ and $n = 1$ states are populated. The difference with the EMD simulation is thus a consequence of the use of only two vibrational states in the MQC simulation. It is expected that this difference will be significant, because for I_2 the equilibrium population of the $n = 2$ vibrational state is ~9%; it is ~3% and ~1% for $n = 3$ and $n = 4$ vibrational states, respectively. Comparing results from the two-level and three-level model simulations in Table 2, it is clear that the VER time is lengthened significantly by including the $n = 2$ state. The VER time increases from 88 to 113 ps and from 114 to 132 ps for the harmonic and anharmonic potentials, respectively. Thus, the MQC simulation with a three-level model yields a VER time in very good agreement with the NEMD results for a harmonic solute and in reasonable agreement for an anharmonic solute.

In addition, from Table 2, for both MQC models, the VER times are significantly longer for the anharmonic solute compared to the harmonic one, which is also observed in the NEMD simulations (see section 4.5).

4.4. Comparison of Different Methods. A comparison of the EMD, NEMD, and MQC results is complicated by a number of issues. First, the overall VER time, T_1, obtained from two-level model MQC simulations cannot be straightforwardly compared to those obtained via the EMD simulations as discussed in section 4.3. The three-level model simulations are presumed to be more directly comparable. Second, the NEMD approach only gives T_1 and no state-to-state information, and under some circumstances, a single time constant such as T_1 is not adequate to represent the energy decay (see Figure 3) for the anharmonic solute. On the other hand, essentially single-exponential decay is observed for the harmonic solute for all initial energies. Third, some of the EMD results rely on the use of QCFs, which are derived on the basis of a harmonic model system[5] and thus are only approximate for the I_2 in Xe system. However, an advantage of this system is that the QCFs are approximately 1 and the classical, mixed quantum−classical, and fully quantum mechanical results are all similar (within 10%).

Given the difficulties just described, the agreement between the relaxation times, T_1, obtained from the low initial energy NEMD and three-level model MQC simulation results is excellent for the harmonic solute potential and reasonable (within ~20−30%) for the anharmonic solute. The relaxation times obtained from the EMD simulations are longer (by ~30%) than the NEMD and MQC times for the harmonic solute. However, the issue can be clarified somewhat by comparing the state-to-state transition rate constants from two-level-model MQC and EMD simulations. The rate constant for the harmonic solute from EMD results, $k_{0\leftarrow 1}^{-1} = 94$ and 102 ps, is in reasonable agreement with that (120 ps) from the MQC two-level model. Assuming the EMD simulation provides a reliable state-to-state rate constant $k_{0\leftarrow 1}$, the VER time $T_1 \approx 69$ and 75 ps is obtained from eq 27 in a two-level system. These values are similar to the $T_1 \approx 88$ ps from MQC simulations for the two-level model. Note however that given the disagreement between the EMD and three-level model MQC T_1 values, it must be that, for the three-level MQC simulations, either (1) the state-to-state rate constant $k_{0\leftarrow 1}$ will not agree with the EMD result or (2) the relation between $k_{0\leftarrow 1}$ and T_1 given in eq 6 does not hold.

Though the relaxation times obtained from the three simulation approaches are in good agreement, the relaxation is several times faster than that observed in the experiments of Paige and Harris.[36] While the experimental energy decay is nonexponential and a single time constant is not sufficient to describe the data, the measured relaxation is clearly much faster than that seen in the simulations. Brown et al. observed this in their NEMD simulations and attributed it to potential functions that are too repulsive[38] (see also refs 10 and 42). We are currently investigating the effect of using improved potential functions to calculate the vibrational relaxation times.

4.5. Comparison of Harmonic and Anharmonic Solutes. The NEMD and MQC simulations provide convenient comparisons of the harmonic and anharmonic solute systems. In the NEMD simulations, the relaxation becomes multiexponential for the anharmonic solute at higher energies but remains single exponential for the harmonic solute. For high initial vibrational excitation, the relaxation is faster in the anharmonic potential than the harmonic potential, as expected. However, the relaxation time, T_1, is longer for the anharmonic solute than the harmonic solute for both NEMD simulations with low initial energies. The same trends are found in the MQC simulations. This is an interesting result though it has been observed previously.[59,60] Of particular note is recent work by Karrlein and Grabert[57] who developed a semiclassical theory of vibrational energy relaxation based on a master equation. The microscopic model that they used is an oscillator coupled to a bath of harmonic oscillators. They found that the VER times are longer for a Morse oscillator than a harmonic oscillator. This is the same trend as we have observed in both the NEMD and MQC simulations. It is important to note that this result applies only to the low initial excitation energies; faster relaxation is still observed (see Figure 3) and expected for high initial energies because of anharmonicity in the vibrational potential.

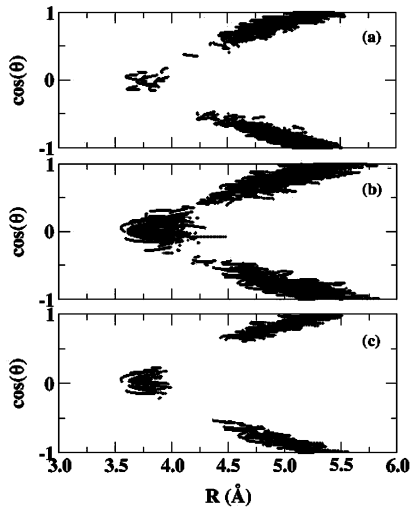

Figure 5. The position distributions of xenon atoms contributing to vibrational relaxation of the I_2 solute (using the anharmonic solute potential). The distributions are given as a function of R, the distance between the xenon atom and I_2 center-of-mass, and θ, the angle between the xenon atom−I_2 center-of-mass vector and the I_2 bond. Each distribution consists of one data point for each time step, representing (a) the xenon atom exerting the largest force along the I_2 bond during a 50 ps EMD simulation, (b) the xenon atom with the largest nonadiabatic coupling contribution during a 50 ps MQC simulation, and (c) the points from panel b with the top 30% nonadiabatic coupling values.

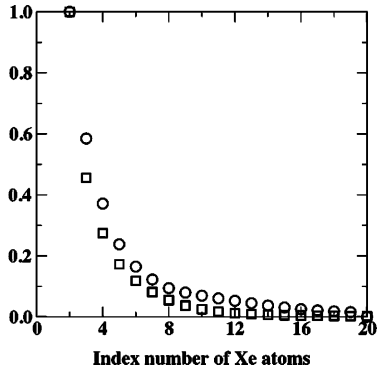

Figure 6. The contribution of individual xenon solvent atoms to the vibrational relaxation: (□) the average of the largest contribution to the nonadiabatic coupling component, $\langle \dot{\mathbf{R}}(i)\cdot\mathbf{d}_{01}(i)\rangle$, obtained from a 50 ps MQC simulation; (○) the average of the force $\langle \mathbf{F}(i)\rangle$ exerted along the I_2 bond by the xenon atom with the largest contribution at each time step in a 50 ps EMD simulation. Only the 20 largest contributions are shown; the averages are normalized to the largest value.

4.6. Mechanistic Information. Both the EMD and MQC simulations are convenient for extracting mechanistic information about the vibrational relaxation. It is interesting to compare the information obtained from the two approaches, and we do so in Figures 5 and 6.

The positions of the solvent xenon atoms that make the biggest contributions to the force, F, along the I_2 bond in a 50 ps EMD simulation are shown in Figure 5a. This clearly shows that most of these solvent atoms are distributed near the two ends of the I_2 molecule. A smaller number are found perpendicular to the I_2 bond with a very short distance from the I_2 center-of-mass. This suggests that the largest solute−solvent interactions, which induce the vibrational energy relaxation, are from the solvent atoms arranged at the ends or very near the center of the I_2 bond. However, this is only an inference because it looks only at the solvent atoms exerting the largest forces while the relaxation time is obtained from the Fourier transform (evaluated at the solute vibrational frequency) of the force autocorrelation function.

Similar results can be obtained from MQC simulations. In Figure 5b, the position distribution is shown of the xenon atoms with the largest nonadiabatic coupling contribution. Results are shown for a 50 ps MQC simulation. This distribution is qualitatively the same as that based on the forces in the EMD simulations but is broader compared to that in Figure 5a. Supposing that only large nonadiabatic coupling is responsible for the vibrational transition, we show in Figure 5c the distribution of the xenon atoms in Figure 5b with the largest 30% nonadiabatic couplings. Obviously this distribution is narrower than that shown in Figure 5b and is centered at slightly smaller center of mass distances.

To estimate how many xenon atoms are involved in the vibrational energy relaxation, the average nonadiabatic coupling component, $\langle \dot{\mathbf{R}}(i)\cdot\mathbf{d}_{01}(i)\rangle$, of each xenon atom i during the MQC simulation and an average force, $\langle \mathbf{F}(i)\rangle$, of each xenon atom i exerted along the bond of I_2 during the EMD simulation are shown in Figure 6. The coupling or force is averaged for the atom with the largest contribution at each time step (the identity of which is not the same at every step), the second largest contribution, and so on. For clarity, results are only shown for the 20 largest contributions. From Figure 6, we can conclude that only a few xenon atoms can participate in the process of energy transfer during the vibrational relaxation. The distribution is slightly broader for the force in the EMD simulation than the coupling in the MQC simulation. Again, the result can be interpreted somewhat more straightforwardly for the MQC simulation because the relaxation time in the EMD simulation is related to the Fourier transform of the force autocorrelation function. The results in Figure 6 support the instantaneous-pair theory analysis of Larsen and Stratt.[42]

5. Concluding Remarks

The vibrational relaxation of I_2 in a xenon solvent has been investigated by three approaches: (1) the standard perturbation theory approach based on equilibrium molecular dynamics (EMD) simulations, (2) classical nonequilibrium molecular dynamics (NEMD) simulations, and (3) mixed quantum−classical (MQC) surface-hopping simulations. Both harmonic and anharmonic I_2 vibrational potentials have been used in these calculations. The vibrational relaxation time, T_1, and the state-to-state rate constants, for example, $k_{0\leftarrow 1}$, have been calculated using each of these methods when possible. In addition, information concerning the mechanisms of vibrational relaxation available from the EMD and MQC simulations has been examined.

The NEMD simulations give relaxation times that are independent of the initial vibrational excitation energy for the harmonic I_2 potential but weakly dependent for the anharmonic potential. If the initial excitation energy is high (6000 or 9000 cm^{-1}), the energy decay is nonexponential for the anharmonic potential and a single time constant such as T_1 is not sufficient to describe the relaxation. In contrast, for the harmonic potential, the energy decay is exponential for all initial energies that we have studied and the relaxation time is essentially constant. Interestingly, for low initial excitation energies (214 and 321 cm^{-1}), the relaxation is slower by ∼50% for the anharmonic I_2 potential than the harmonic potential, which is in good agreement with Karrlein and Grabert's calculated VER rates at low excitation energy[57] and previous gas-phase calculations.

To obtain the perturbation theory results from the EMD simulations, we use the quantum correction factor for a harmonic

solute bilinearly coupled to a harmonic bath.[5] For this system, the quantum correction factor is ~1.08, and therefore, the classical, quantum, and mixed quantum−classical perturbation theory approaches give similar results. The relaxation lifetimes for the harmonic potential are significantly longer (by ~20−30%) than those from the NEMD simulations. If it is assumed that the harmonic potential results can be used also for the anharmonic case, quite good agreement with the NEMD calculations is found.

We have investigated two short-time approximations to the force autocorrelation function obtained in the EMD simulations that are frequently used in calculating relaxation times. The Gaussian approximation gives significant error, resulting in a relaxation time that is too long by a factor of ~50. Significant improvement is obtained with a fit of order t^4,[8] giving a result within a factor of 3 of the numerically calculated T_1.

The MQC simulations have been carried out using two-level and three-level models. The two-level model gives unreliable T_1 values, but the state-to-state rate constant, $k_{0\leftarrow1}$, obtained for the harmonic potential is in reasonable agreement with that from the EMD simulations. The three-level model gives relaxation times that are in excellent agreement with the NEMD calculations for the harmonic I_2 potential and in reasonable agreement for the anharmonic potential. The MQC results give longer relaxation times for the anharmonic potential than the harmonic potential, in agreement with the NEMD results.

An analysis of mechanistic information from both the EMD and MQC simulations indicates that (1) only one or two xenon atoms are primarily involved in the vibrational relaxation and (2) the most effective position for a xenon atom for promoting energy transfer is near the ends of the I_2 molecule or very near the center-of-mass. The two approaches give qualitatively and semiquantitatively similar results in both regards.

The present results provide an interesting comparison of different methods for simulating vibrational relaxation in a realistic system in which quantum effects are expected to be small. Overall, the three methods studied here are in relatively good agreement with differences only on the order of ~10−50% in T_1 and $k_{0\leftarrow1}$. This is expected for a low-frequency solute such as I_2, though there are few direct comparisons of different approaches (especially the surface-hopping method). The relaxation is much too fast (by a factor of ~10) relative to experiments,[36] which is likely due to the potential used.[38] Clearly, different implementations of the mixed quantum−classical treatment, that is, in the context of perturbation theory or in a nonequilibrium surface-hopping approach, do not give the same relaxation time; how these approaches behave in cases in which quantum mechanical effects are important, for example, relaxation of a higher frequency solute, is currently under investigation.

Acknowledgment. The authors thank Dr. Yao Houndonougbo for useful discussions. Acknowledgment is made to the donors of the Petroleum Research Fund, administered by the ACS, for support of this research. The computer facilities of the Kansas Center for Advanced Scientific Computing were used to carry out some of the calculations.

References and Notes

(1) Oxtoby, D. W. *Adv. Chem. Phys.* **1981**, *47*, 487.
(2) Owrutsky, J. C.; Raftery, D.; Hochstrasser, R. M. *Annu. Rev. Phys. Chem.* **1994**, *45*, 519.
(3) Gnanakaran, S.; Hochstrasser, R. M. *J. Chem. Phys.* **1996**, *105*, 3486.
(4) Zhang, Q.; Baronavski, A. P.; Qwrutsky, J. C. *J. Chem. Phys.* **2003**, *118*, 7074.
(5) Bader, J. S.; Berne, B. J. *J. Chem. Phys.* **1994**, *100*, 8359.
(6) Egorov, S. A.; Rabani, E.; Berne, B. J. *J. Phys. Chem. B* **1999**, *103*, 10978.
(7) Everitt, K. F.; Skinner, J. L. *J. Chem. Phys.* **1999**, *110*, 4467.
(8) Egorov, S. A.; Skinner, J. L. *J. Chem. Phys.* **1996**, *105*, 7047.
(9) Egorov, S. A.; Everitt, K. F.; Skinner, J. L. *J. Phys. Chem. A* **1999**, *103*, 9494.
(10) Everitt, K. F.; Egorov, S. A.; Skinner, J. L. *Chem. Phys.* **1998**, *235*, 115.
(11) Everitt, K. F.; Skinner, J. L.; Ladanyi, B. M. *J. Chem. Phys.* **2002**, *116*, 179.
(12) Skinner, J. L. *J. Chem. Phys.* **1997**, *107*, 8717.
(13) Skinner, J. L.; Park, K. *J. Phys. Chem. B* **2001**, *105*, 6716.
(14) Egorov, S. A.; Berne, B. J. *J. Chem. Phys.* **1997**, *107*, 6050.
(15) Egorov, S. A.; Skinner, J. L. *J. Chem. Phys.* **1997**, *106*, 1034.
(16) Whitnell, R. M.; Wilson, K. R.; Hynes, J. T. *J. Phys. Chem.* **1990**, *94*, 8625.
(17) Whitnell, R. M.; Wilson, K. R.; Hynes, J. T. *J. Chem. Phys.* **1992**, *96*, 5354.
(18) Rey, R.; Hynes, J. T. *J. Chem. Phys.* **1998**, *108*, 142.
(19) Adelman, S. A.; Stote, R. H. *J. Chem. Phys.* **1988**, *88*, 4397.
(20) Miller, D. W.; Adelman, S. A. *J. Chem. Phys.* **2002**, *117*, 2672.
(21) Miller, D. W.; Adelman, S. A. *J. Chem. Phys.* **2002**, *117*, 2688.
(22) Adelman, S. A.; Muralidhar, R.; Stote, R. H. *J. Chem. Phys.* **1991**, *95*, 2738.
(23) Heidelbach, C.; Vikhrenko, V. S.; Schwarzer, D.; Fedchenia, I. I.; Schroeder, J. *J. Chem. Phys.* **1999**, *111*, 8022.
(24) Chesnoy, J.; Gale, G. M. *Ann. Phys.* **1984**, *9*, 893.
(25) Morita, A.; Kato, S. *J. Chem. Phys.* **1998**, *109*, 5511.
(26) Kim, H.; Rossky, P. J. *J. Phys. Chem. B* **2002**, *106*, 8240.
(27) Voth, G. A. *Adv. Chem. Phys.* **1996**, *93*, 135.
(28) Poulsen, J.; Keiding, S. R.; Rossky, P. J. *Chem. Phys. Lett.* **2001**, *336*, 488.
(29) Reichman, D. R.; Roy, P. N.; Jang, S.; Voth, G. A. *J. Chem. Phys.* **2000**, *113*, 919.
(30) Gai, H.; Voth, G. A. *J. Chem. Phys.* **1993**, *99*, 740.
(31) Figueirido, F. E.; Levy, R. M. *J. Chem. Phys.* **1992**, *97*, 703.
(32) Vikhrenko, V. S.; Heidelbach, C.; Schwarzer, D.; Nemtsov, V. B.; Schroeder, J. *J. Chem. Phys.* **1999**, *110*, 5273.
(33) Heidelbach, C.; Vikhrenko, V. S.; Schwarzer, D.; Schroeder, J. *J. Chem. Phys.* **1999**, *110*, 5286.
(34) Hammes-Schiffer, S.; Tully, J. C. *J. Chem. Phys.* **1994**, *101*, 4657.
(35) Tully, J. C. *J. Chem. Phys.* **1990**, *93*, 1061.
(36) Paige, M. E.; Harris, C. B. *Chem. Phys.* **1990**, *149*, 37.
(37) Paige, M. E.; Russell, D. J.; Harris, C. B. *J. Chem. Phys.* **1986**, *85*, 3699.
(38) Brown, J. K.; Harris, C. B.; Tully, J. C. *J. Chem. Phys.* **1988**, *89*, 6687.
(39) Nesbitt, D. J.; Hynes, J. T. *Chem. Phys. Lett.* **1981**, *82*, 252.
(40) Nesbitt, D. J.; Hynes, J. T. *J. Chem. Phys.* **1982**, *76*, 6002.
(41) Stote, R. H.; Adelman, S. A. *J. Chem. Phys.* **1988**, *88*, 4415.
(42) Larsen, R. E.; Stratt, R. M. *J. Chem. Phys.* **1999**, *110*, 1036.
(43) The experimental energy decay is nonexponential, and thus, strictly speaking, there is not a well-defined T_1.
(44) Landau, L. D.; Teller, E. A. *Phys. Z. Sowjetunion* **1936**, *10*, 34.
(45) Bastida, A.; Zuniga, J.; Requena, A.; Halberstadt, N.; Beswick, J. A. *J. Chem. Phys.* **1998**, *109*, 6320.
(46) Bastida, A.; Miguel, B.; Zuniga, J.; Requena, A.; Halberstadt, N.; Janda, K. C. *J. Chem. Phys.* **1999**, *111*, 4577.
(47) Bastida, A.; Zuniga, J.; Requena, A.; Halberstadt, N.; Beswick, J. A. *PhysChemComm* **2000**, *7*.
(48) Herman, M. F. *J. Chem. Phys.* **1987**, *87*, 4794.
(49) Thompson, W. H. *J. Chem. Phys.* **2003**, *118*, 1059.
(50) Bittner, E. R.; Rossky, P. J. *J. Chem. Phys.* **1995**, *103*, 8130.
(51) Schwartz, B. J.; Bittner, E. R.; Prezhdo, O. V.; Rossky, P. J. *J. Chem. Phys.* **1996**, *104*, 5942.
(52) Allen, M. P.; Tildesley, D. J. *Computer simulation of liquids*; Oxford science publictions: Oxford, U.K., 1987.
(53) Lanczos, C. *J. Res. Natl. Bur. Stand.* **1950**, *45*, 255.
(54) Saad, Y. *Numerical Methods for Large Eigenvalue Problems*; Halstead: New York, 1992.
(55) Echave, J.; Clary, D. C. *Chem. Phys. Lett.* **1992**, *190*, 225.
(56) Wei, H.; Carrington, T. J. *J. Chem. Phys.* **1992**, *97*, 3029.
(57) Karrlein, R.; Grabert, H. *J. Chem. Phys.* **1998**, *108*, 4972.
(58) Frost, A. A.; Pearson, R. G. *Kinetics and mechanism*; John Wiley & Sons, Inc.: New York, London, 1963.
(59) Mies, H. F. *J. Chem. Phys.* **1964**, *40*, 523.
(60) Taylor, A. J.; Cianturco, F. A. *Chem. Phys. Lett.* **1969**, *4*, 376.